

LM-GAN: A Photorealistic All-Weather Parametric Sky Model

LUCAS VALENÇA, Université Laval, Canada
 IAN MAQUIGNAZ, Université Laval, Canada
 HADI MOAZEN, Université Laval, Canada
 RISHIKESH MADAN, Université Laval, Canada
 YANNICK HOLD-GEOFFROY, Adobe Research, USA
 JEAN-FRANÇOIS LALONDE, Université Laval, Canada



Fig. 1. For an input parametric sky (left, inset), our method generates a photorealistic, all-weather HDR environment map (right, inset) while coherently preserving the parametric sky’s illumination. This mapping is achieved by combining a generative adversarial pipeline with a differentiable rendering loss. Scene from Blender Studio under CC0 license with added reflective surfaces.

We present LM-GAN, an HDR sky model that generates photorealistic environment maps with weathered skies. Our sky model retains the flexibility of traditional parametric models and enables the reproduction of photorealistic all-weather skies with visual diversity in cloud formations. This is achieved with flexible and intuitive user controls for parameters, including sun position, sky color, and atmospheric turbidity. Our method is trained directly from inputs fitted to real HDR skies, learning both to preserve the input’s illumination and correlate it to the real reference’s atmospheric components in an end-to-end manner. Our main contributions are a generative model trained on both sky appearance and scene rendering losses, as well as a novel sky-parameter fitting algorithm. We demonstrate that our fitting algorithm surpasses existing approaches in both accuracy and sky fidelity, and also provide quantitative and qualitative analyses, demonstrating LM-GAN’s ability to match parametric input to photorealistic all-weather skies. The generated HDR environment maps are ready to use in 3D rendering engines and can be applied to a wide range of image-based lighting applications.

1 INTRODUCTION

Natural illumination is a key component of photorealism, with a pronounced impact on human perception. It is a significant aspect of the design of physical spaces, the planning of urban architecture, and even the perceived visual quality of media & film. The rendering of photorealistic illumination for virtual scenes is generally achieved through the adoption of high dynamic range (HDR) environment maps to guide Image-Based Lighting (IBL) techniques [Debevec 1998]. Either physically captured or synthetically generated, HDR

imagery (HDRI) is generally understood to represent a hemispherical map of a desired sky dome, projected to a skybox, equirectangular, or other textural representation. Though conventional low dynamic range (LDR) imagery can be suitable for environment mapping, HDR imaging is integral to the photorealistic rendering of outdoor scenes. For physical HDR captures, an estimated 22 f-stops of exposure are necessary to fully faithfully capture outdoor illumination [Stumpfel et al. 2006]. While HDR imaging of real skies is unsurpassed in the photorealism of its output, it is an inflexible solution, as captures are of specific, uncontrolled scene configurations.

To overcome the rigidity of physical capture, parametric sky models have progressed greatly over the past four decades. Originally targeting scientific and engineering applications (e.g., [Moon 1940; Perez et al. 1993] model only luminance), Nishita et al. [1993] proposed the first color model, with the goal of enabling the rendering of extraterrestrial views of the Earth for space flight simulators. This model was then extended to include multiple scattering events within the atmosphere, primitive clouds [Nishita et al. 1996], and later reduced via non-linear least squares fitting by Preetham et al. [1999]. In order to achieve better accuracy while reducing computational time and memory footprint, these models have evolved to the incumbent Hošek-Wilkie-based series of models [2012; 2013; 2022; 2021]. These are mathematical approximations fitted to data from physical simulations, later validated against real captured skies. While these models show great physical accuracy, they can only properly approximate ideal homogeneous skies, devoid of non-uniform atmospheric formations such as clouds.

In recent years, the advent of deep learning has led to the proposal of deep sky models, with the capacity to self-discover features

Authors’ addresses: Lucas Valença, Université Laval, Canada, lucas.valenca@ulaval.ca; Ian Maquignaz, Université Laval, Canada, ian.maquignaz.1@ulaval.ca; Hadi Moazen, Université Laval, Canada, hadi.moazen.1@ulaval.ca; Rishikesh Madan, Université Laval, Canada, rishikesh.madan.1@ulaval.ca; Yannick Hold-Geoffroy, Adobe Research, USA, holdgeof@adobe.com; Jean-François Lalonde, Université Laval, Canada, jean-francois.lalonde@gel.ulaval.ca.

and modalities through latent parameters. Notably, this concept has been demonstrated for lighting estimation [Hold-Geoffroy et al. 2019, 2017; Yu et al. 2021a; Zhang et al. 2019b], where LDR images can be used to guide the generation of HDR environment maps for relighting virtual objects and scenes. Though these learned representations tend to offer little photorealism and generate overly smooth skies, they capture lighting energy with significant accuracy. Recently, generative adversarial networks (GANs) targeted towards reproducing clouds have been proposed [Hojdar 2019; Mirbauer et al. 2022; Satilmis et al. 2022], but these either fail to capture photorealistic textures or lack full HDR capabilities.

In this work, we propose a learned sky model capable of producing photorealistic weathered skies with faithful and controllable HDR illumination. Our method combines the versatility of parametric models and the realism of deep generative networks. We leverage the Lalonde-Matthews (LM) parametric illumination model [Lalonde and Matthews 2014], which represents outdoor skies with parameters such as sun position, sky color, and atmospheric turbidity. This model is also particularly suitable to model overcast skies, having been previously used to guide a state-of-the-art all-weather deep lighting estimation approach [Zhang et al. 2019b]. Given a set of such parameters, we first render a sky dome using the LM equation (see sec. 3.1) and feed the resulting HDR image as input to a deep convolutional network, trained in an adversarial setting on over 25,000 HDR skydomes from the publicly-available Laval HDR Sky Dataset [Lalonde et al. 2016; Lalonde and Matthews 2014]. The resulting network, dubbed *LM-GAN*, can be controlled using the same parameters to produce photorealistic weathered HDR skies, which can readily be used in any existing physics-based rendering engine (see fig. 1). We demonstrate through quantitative evaluations and ablation studies that our proposed LM-GAN retains parametric fidelity to the LM model and surpasses the current state-of-the-art learning-based models in versatility, fidelity, and photorealism.

2 RELATED WORK

Early models of solar and atmospheric illumination such as [Moon 1940] and [Perez et al. 1993] were oriented towards scientific and engineering applications. With the advent of the digital age, Image-Based Lighting (IBL) techniques [Debevec 1998] proposed the use of High Dynamic Range Imagery (HDRI [Reinhard et al. 2010]) to render synthetic objects into real and virtual scenes. This new paradigm of applications spurred renewed interest in modeling skies and alleviating the burden of physical capture.

2.1 Parametric models

To limit the computational resources required to model sunlight and skylight, it is often preferable to approximate its appearance via a mathematical model and evaluate it against physically captured skies [Kider et al. 2014]. One such formulation is through the development of numerical models such as [Bruneton and Neyret 2008; Elek and Kmoch 2010; Haber et al. 2005; Nishita et al. 1996, 1993; O’Neil 2005], which derive simplified mathematical representations for complex atmospheric systems. Though reducing computation expense, numerical models generally remain complex, memory intensive, and require a pre-computation step.

An alternative formulation introduced by Perez et al. [1993] is the fitting of an analytical model to a body of sky data. These simpler models can be fitted to computationally expensive, accurate, and diverse data acquired from complex models (e.g., Preetham et al. [1999] is fitted to [Nishita et al. 1996]), path tracers [Hošek and Wilkie 2012, 2013; Wilkie et al. 2021], or physical simulations such as libRadtran [Emde et al. 2016] (as used in evaluation by Bruneton [Bruneton 2017]). Such models trade-off accuracy to produce lightweight, flexible, and fast parametric models which support a wide range of applications [Bruneton 2017].

2.2 Synthetic cloud generation

Though allowing for versatility through a finite set of intuitive parameters, parametric models are generally limited to clear, hazy, and overcast skies. To include more complex atmospheric formations such as clouds, parametric models are often supplemented by volumetric cloud rendering [Kallweit et al. 2017] and/or cloud simulations [Bouthors et al. 2008] through various proposed implementations. While this combined approach can be versatile and photorealistic, it can be labor intensive, computationally expensive and difficult to configure [Hill et al. 2020].

2.3 Learned parametric models

Recently, deep learning methods have been proposed for lighting estimation and the fitting of skies to lighting models. Works such as [Hold-Geoffroy et al. 2017; Zhang et al. 2019b] enable HDR relighting of virtual objects/scenes by regressing the parameters of parametric lighting models ([Hošek and Wilkie 2012; Lalonde and Matthews 2014], respectively) from singular, limited field of view LDR images. Other approaches [Hold-Geoffroy et al. 2019; Yu et al. 2021a,b] focus on learning the illumination model itself. These methods offer high fidelity for relighting photographs, but do not obtain photorealistic textures, aiming instead at better generalization on the previously-mentioned challenges.

Most recently, approaches have been proposed to augment parametric skies with photorealistic clouds. Satilmis et al. [2022] proposed a method for augmenting Hošek-Wilkie [2012] parametric skies per user-controlled cloud placement. This differs from our model in that the user is required to provide a mask positioning the cloud textures, whereas we wish to have clouds naturally positioned as a direct consequence of a learned mapping from parametric inputs to the real world. SkyGAN [Mirsauer et al. 2022] proposed fitting the Prague sky model [2021] model to real-world photographs, enabling the re-generation of Prague skies with atmospheric formations, though with limited dynamic range, thus requiring an extra virtual sun lamp to be used with rendered scenes. To the best of our knowledge, LM-GAN is the first to produce parametric, photorealistic all-weather HDR skydomes for Image-Based Lighting.

3 METHOD

We briefly summarize our model below and discuss the fitting of the Lalonde-Matthews (LM) model parameters to HDR imagery. In this work, we leverage physically captured images from the publicly-available *Laval HDR Sky Dataset* [Lalonde et al. 2016].

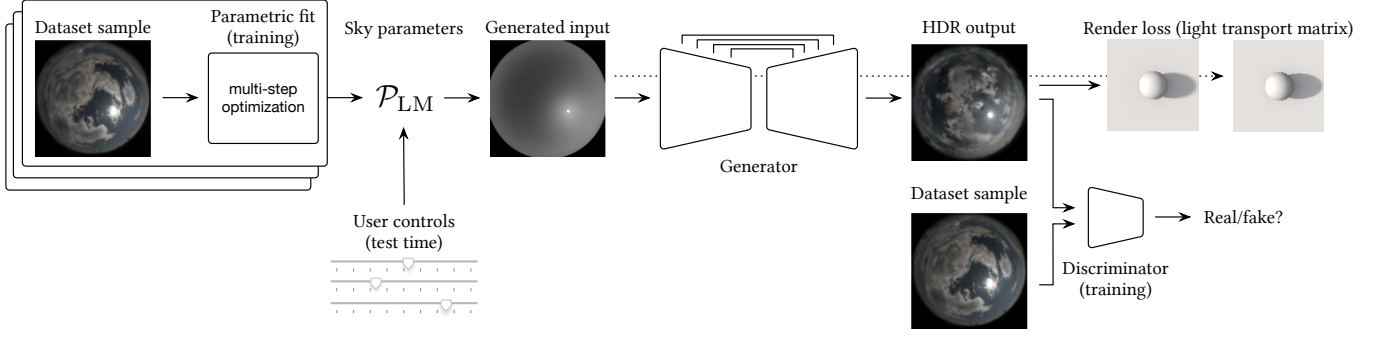


Fig. 2. **Our pipeline.** A generator is trained to convert a parametric input (obtained by fitting a parametric model to a captured HDR sky) to a photorealistic weathered HDR sky via a combination of a patch-based discriminator (GAN) loss, LPIPS (not shown), and a differentiable rendering loss.

3.1 Representing real skies parametrically

Where previous works such as [Hold-Geoffroy et al. 2017; Mirbauer et al. 2022] have used the Hošek-Wilkie model [2012], we leverage the LM [2014] illumination model instead. This model offers 11 parameters for approximating outdoor lighting which can be fit to real HDR skies. It is also less restrictive in its parameters than traditional physically-based models, having thus been shown to be well-suited for learning-based approaches [Lalonde and Matthews 2014; Zhang et al. 2019b].

The Lalonde-Matthews (LM) model. The LM model is a hemispherical function of an arbitrary light direction \mathbf{l} (in spherical coordinates) and can be written compactly as the sum of two terms:

$$f_{LM}(\mathbf{l}; \mathcal{P}_{LM}) = f_{sun}(\mathbf{l}; \mathcal{P}_{sun}, \mathbf{l}_{sun}) + f_{sky}(\mathbf{l}; \mathcal{P}_{sky}, \mathbf{l}_{sun}) \quad (1)$$

Where $\mathbf{l}_{sun} = [\theta_{sun}, \varphi_{sun}]$ is the sun angular position in spherical coordinates, and \mathcal{P}_* represent term-specific parameters. The sky term f_{sky} in eq. (1) is the Preetham [1999] sky model f_{Pre} , parameterized by turbidity t and multiplied channel-wise with an average sky color $\mathbf{c}_{sky} \in \mathbb{R}^3$:

$$f_{sky}(\mathbf{l}; \mathcal{P}_{sky}, \mathbf{l}_{sun}) = \mathbf{c}_{sky} f_{Pre}(\theta_{sun}, \gamma_{sun}, t) \quad (2)$$

Where γ_{sun} is the angle between sky direction \mathbf{l} and the sun \mathbf{l}_{sun} . The sun term f_{sun} in eq. (1) is defined as:

$$f_{sun}(\mathbf{l}; \mathcal{P}_{sun}, \mathbf{l}_{sun}) = \mathbf{c}_{sun} \exp(-\beta \exp(-\kappa/\gamma_{sun})) \quad (3)$$

Where (β, κ) control the sun scattering, and $\mathbf{c}_{sun} \in \mathbb{R}^3$ is the mean sun color. To summarize, the LM model represents the HDR sky dome with the following 11 parameters:

$$\mathcal{P}_{LM} = \{\mathbf{c}_{sky}, t, \mathbf{c}_{sun}, \beta, \kappa, \mathbf{l}_{sun}\} \quad (4)$$

LM fitting algorithm. Similar to [Lalonde and Matthews 2014], we employ an optimization scheme to fit LM parameters to captured HDR hemispherical skies. We assume the sun position \mathbf{l}_{sun} can be obtained from capture metadata (geolocation and timestamp) and fine-tuned with a simple local maximum energy search (on patches, to handle overcast scenarios). We then initialize both \mathbf{c}_{sun} and \mathbf{c}_{sky} to the target sky image’s mean color. This is achieved by masking a 30° circular region around the sun, sufficient for both sunny and overcast skies. We also exclude suns over 80° of zenith, as those

skies tend to lack sufficient daylight due to geographic reasons. Fitting is achieved through the following 4-step strategy:

- (1) A coarse grid-search to initialize scattering parameter κ . In this step, we employ a coarse grid, consisting of s_κ steps within a range of $[\kappa_{min}, \kappa_{max}]$, combined with standard steps S for both $\beta \in [\beta_{min}, \beta_{max}]$ and $t \in [t_{min}, t_{max}]$. We employ two losses: (a) An L1 smoothing loss; between the generated LM sky and target HDR image (b) An L1 rendering loss; between the generated LM sky and target HDR image after transformation by a pre-computed light transport matrix [Sloan et al. 2002] onto a scene composed of a Lambertian diffuse sphere and ground plane (see fig. 2).
- (2) A fine grid-search to determine scattering parameters κ , β , and t . The same L1 losses are used. In this step, κ is initialized to the best result of the previous step, now with s_κ steps scaled by λ_κ , in a proportionally smaller range extending in both directions. Parameters β and t are iterated as before. The best combination for all 3 parameters is stored.
- (3) Optimization of the ω_{sun} and ω_{sky} parameters via the Adam optimizer [Kingma and Ba 2015] with frozen scattering parameters κ , β , and t for n iterations. The same L1 losses are used, with added fixed regularization penalties when either the sun or sky color collapses to zero (or an extreme value), and when the color of the sun or sky is neither approximately grayscale, red, or blue (the latter, for skies only).
- (4) Iterative fine-tuning of all parameters (except sun positioning) with the Adam optimizer, for n more epochs. Regularization and losses are carried forward from Step 3. For reproducibility and details on constants and ranges, see sec. 3.3.

Using this 4-step strategy, we have annotated over 25,000 skies from the *Laval HDR Sky Dataset*.

3.2 Generating photorealistic skies

As illustrated in fig. 2, our generative pipeline takes as input a sky dome (c.f. sec. 3.1), generated from either user-specified parameters or a real sky. Then, our model generates a photorealistic weathered sky which preserves the input’s HDR illumination.

Preserving HDR illumination. To preserve the dynamic range, the model’s inputs are pre-processed to compressed towards the $[-1, 1]$

interval preferred by the model architecture. This is achieved by (1) re-exposing input skies by dividing by their respective 99th percentile, (2) tonemapping by $I' = \log_2(I + 1)$, and, (3) shifting inputs towards the $[-1, 1]$ interval with $I' = 2I - 1$. Post-generation, this procedure is inverted to recover the dynamic range. Through Figure fig. 4, we demonstrate this process preserves the dynamic range of the input’s illumination.

Network architecture. The model consists of a UNet [Ronneberger et al. 2015] with fixed update initialization [Zhang et al. 2019a] and ReLU activation. Dropout [Srivastava et al. 2014] is enabled in the bottleneck during training and testing for increased generalization [Isola et al. 2017]. The model halves the resolution and doubles the features at every *down layer*. For an input $s \times s$ image, it has $(\log_2(s) - 2)$ *down layers*, ensuring a 4×4 resolution at the bottleneck with $2s$ filters. Training data is augmented via x and y -axes flips and azimuthal rotations, which encourages the network to learn multiple variations of the same sky.

Loss functions. During training, the network combines three loss functions: patch-based adversarial [Isola et al. 2017], LPIPS perceptual [Zhang et al. 2018], and a rendering loss. For more details on how each loss contributes to the generated result, see sec. 4.3.

The main texture loss is a simple PatchGAN [Isola et al. 2017] loss, directly calculated as an MSE from the output patch feature vectors of a patch-based discriminator with a receptive field of 8×8 pixels. The discriminator employs ReLU activations—except for a sigmoid at the end—and instance normalization throughout. Because the goal is to learn general texture and structure, every input given to the discriminator is tonemapped as above.

To further encourage the modeling of details and high frequencies, we also employ an LPIPS [Zhang et al. 2018] perceptual loss of a VGG [Simonyan and Zisserman 2015] network trained on ImageNet [Deng et al. 2009]. This loss has been observed to learn cloud texture details (see fig. 5). As with the generator, this network receives tonemapped images. This loss is scaled so its magnitude is generally 10 times smaller than the PatchGAN loss, so that it is only given attention during training after the network learned the general structure of the model.

To ensure lighting is preserved, the output of the generator is converted back to linear RGB and used to render a diffuse white sphere on a plane using a light transport matrix (as in sec. 3.1), which is used to calculate a differentiable rendering L1 loss against the same scene lit by the linear LM parametric input. The magnitude of this loss is scaled to be 10 times smaller than the LPIPS loss, so that emphasis to coherent lighting is only enforced when the visuals are more well-behaved, otherwise HDR artifacts can appear.

3.3 Implementation details

Our implementation uses PyTorch and was based on UNet FixUp [Griffiths et al. 2022] and adapted to our generative scenario. The light transport rendering engine and LM rendering engine, as well as the LM fitting algorithm, are all PyTorch scripts vectorized and with GPGPU. Models were trained until convergence (around 440 epochs), with batch sizes chosen as the highest value to fit the GPU used for training. On a single Titan X GPU, the 128×128 models took

on average 15 minutes per epoch to train and consuming 11 GB of VRAM on a batch size of 32. For the fitting algorithm, we employed the search ranges for (κ, β, t) as $[0, 1]$, $[0, 50]$, $[2, 20]$, respectively, determined empirically by finding points where the model became incoherent. Our search used $s_\kappa = \lambda_\kappa = 0.1$, with $S = 2$ and $n = 1000$.

4 EXPERIMENTS

We compare our technique to the state of the art, both in terms of sky appearance and HDR lighting fidelity. We also evaluate how well our parametric fitting compares to state-of-the-art fitting approaches.

4.1 Methodology

Dataset. We employ the Laval HDR Skies dataset [Lalonde et al. 2016] to evaluate all methods, from which we sample a test set that was not accessible during training (c.f. sec. 3.1). For evaluation we bin this test set by NOAA forecast weather descriptions [Oceanic and Administration 2023], first using color-based binary thresholding [Heinle et al. 2010]. By counting the percentage of cloud coverage, we classify the test set as follows: 0–1/8 of the sky covered by clouds is named a *sunny* sky (su), 1/8–3/8 *mostly sunny* (ms), 3/8–5/8 *partly cloudy* (pc), 5/8–7/8 *mostly cloudy* (mc), and 7/8–1 *overcast* (oc). Moreover, we also separate the skies where the sun is within 20° of the horizon as a *sunrise/sunset* (ss) category, due to their different color and lighting configurations. To ensure the train and test sets do not share time-adjacent frames, the test set is composed of completely separate days of capture, never seen in training. Each day in the test set is from approximately a different month, resulting in 2,580 samples completely separate from the dataset’s remaining 23,000. The final distribution per bin in the test set is 565 sunny, 534 mostly sunny, 380 partly cloudy, 375 mostly cloudy, 396 overcast, 330 sunrise/sunset.

Metrics. To evaluate the appearance and diversity of sky models, we use the FID measure [Heusel et al. 2017] to compare their distributions of appearance. Prior to computing the FID, skies are re-exposed to their 99th percentile, then applied a $\gamma = 2.2$ tone mapping and finally clamped to a range between 0 and 1. We further consider the RMSE metric and its scale-invariant counterpart, si-RMSE [Grosse et al. 2009], computed on the generated skies. The former captures the absolute amount of energy present in the sky, penalizing a lack of strong sun values, while the latter compensates for intensity mismatches and focuses on correct contrast. We compute the RMSE/si-RMSE scores on a Lambertian diffuse scene rendered with a precomputed transport matrix (c.f. sec. 3.1).

Parametric models. We first consider three parametric sky models: the combined sun and sky Hošek-Wilkie [2013] (fit using the algorithm of [Hold-Geoffroy et al. 2017]); its extension, the “Prague Sky Model” [Wilkie et al. 2021] (fit using the algorithm of [Mirbauer et al. 2022]); and the Lalonde-Matthews [2014] (fit by our custom algorithm, see sec. 3.1). All parametric models are optimized to our HDR test set.

Learned models. We also compare against the deep sky model SkyNet [Hold-Geoffroy et al. 2019] trained on the same dataset as our model; and the current state-of-the-art neural sky model, SkyGAN [Mirbauer et al. 2022], which we re-implemented from the information

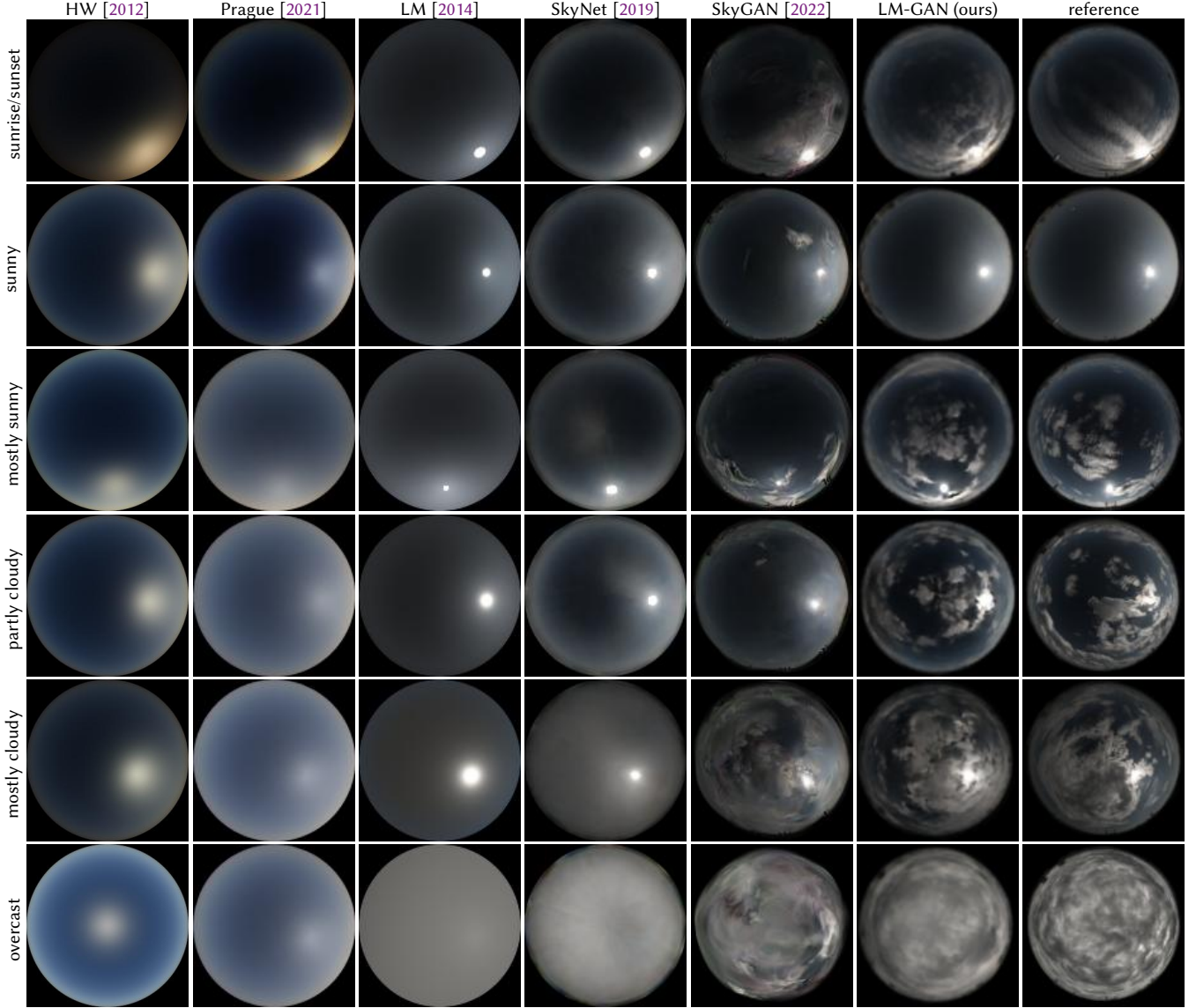


Fig. 3. **Visual comparison of different sky lighting models.** While physics-based parametric models ([Hošek and Wilkie 2012], [Wilkie et al. 2021]) are physically accurate, they fail to accurately represent skies with diverse atmospheric conditions, such as clouds. The LM [2014] and SkyNet [2019] models are more versatile but yield oversmooth results. SkyGAN [2022] generates somewhat unrealistic clouds. In contrast, our approach maintains the versatility of parametric models and the photorealism of photographic reference.

provided in the paper and also trained on the same dataset as ours, using the aforementioned Hošek-Wilkie fits as input.

SkyGAN relies on StyleGAN3 [Karras et al. 2021] and also produces a realistic sky given a parametric input. However, SkyGAN produces a residual, which is *added* to the parametric input. We also observe, as in [Mirbauer et al. 2022], that it is not able to preserve HDR lighting from the input.

4.2 HDR sky synthesis

Quantitative evaluation. We first compare all techniques on our HDR environment map test set in skyangular format in tab. 1. We observe that increasing the cloud coverage significantly worsens the FID of parametric sky models—attaining an FID of over 200. In comparison, our method achieves consistent robustness, down to a value of 20.28 on the entire test set’s distribution, and 38.46 in the worst case. Overall, the RMSE measure tells a different story, where increasing cloud coverage provides lower error, as the amount of

	model	su	ms	pc	mc	oc	ss	all
FID	HW [2013]	142.83	200.17	208.81	202.53	175.36	188.08	175.29
	Prague [2021]	170.32	228.89	233.84	224.49	195.52	207.79	202.46
	LM [2014]	147.13	190.72	205.27	197.36	174.02	178.06	169.95
	SkyNet [2019]	126.24	187.22	209.72	214.07	190.65	167.61	165.83
	SkyGAN [2022]	40.95	38.94	46.27	55.12	71.23	73.96	34.89
	LM-GAN (ours)	29.57	28.03	29.15	30.38	38.59	38.46	20.28
RMSE	HW [2013]	29.02	19.74	12.78	5.75	2.89	7.89	14.61
	Prague [2021]	29.02	19.75	12.81	5.79	2.92	7.9	14.63
	LM [2014]	22.48	13.25	9.36	5.74	3.83	7.66	11.45
	SkyNet [2019]	26.62	18.24	12.79	6.27	2.71	7.84	13.82
	SkyGAN [2022]	28.98	19.72	12.77	5.73	2.86	7.86	14.59
	LM-GAN (ours)	21.71	12.56	8.70	4.97	3.16	7.18	10.76
si-RMSE	HW [2013]	28.99	19.72	12.76	5.73	2.87	7.86	14.59
	Prague [2021]	29.02	19.74	12.78	5.75	2.89	7.89	14.62
	LM [2014]	20.18	11.43	7.50	3.31	1.43	6.59	9.43
	SkyNet [2019]	25.08	16.76	10.96	5.01	2.43	7.02	12.58
	SkyGAN [2022]	28.64	19.57	12.72	5.71	2.84	7.66	14.44
	LM-GAN (ours)	19.72	11.08	7.30	3.16	1.37	6.31	9.17

Table 1. **Error on the sky texture.** The columns indicate the splits according to cloudiness (c.f. sec. 4.1), ranging from sunny (su) to overcast (oc), and sunrise/sunset (ss). “all” indicates metrics averaged over the entire test set.

	model	su	ms	pc	mc	oc	ss	all
RMSE (ref.)	HW [2013]	6417.78	4431.04	3138.49	2193.35	1898.95	1529.03	3591.46
	Prague [2021]	4767.83	3180.79	2348.25	1484.03	1248.14	1098.06	2596.64
	LM [2014]	1163.16	716.64	582.67	407.78	320.21	120.11	612.84
	SkyNet [2019]	2596.66	2236.56	2276.70	1562.40	970.81	995.53	1870.67
	SkyGAN [2022]	6235.02	4375.28	2959.59	1858.38	1432.77	1448.21	3382.92
	LM-GAN (ours)	1175.01	707.38	571.89	402.45	308.04	125.21	609.94
si-RMSE (ref.)	HW [2013]	2158.68	1591.31	1078.51	742.31	825.80	547.31	1265.88
	Prague [2021]	1958.56	1461.44	1150.64	918.86	895.20	509.38	1237.26
	LM [2014]	158.29	113.75	107.58	117.70	120.09	66.46	118.12
	SkyNet [2019]	311.97	284.94	238.47	196.44	144.37	177.05	235.80
	SkyGAN [2022]	1278.86	870.70	529.37	285.27	224.39	363.76	660.79
	LM-GAN (ours)	171.05	121.78	112.15	117.28	115.81	62.82	122.06
RMSE	SkyGAN [2022]	506.93	526.74	606.77	742.99	1028.20	574.81	648.77
	LM-GAN (ours)	234.16	170.08	139.93	104.94	84.46	55.40	142.43
si-RMSE	SkyGAN [2022]	319.59	329.63	360.12	381.01	484.37	313.51	361.10
	LM-GAN (ours)	95.53	78.62	69.46	58.94	53.88	42.03	69.65

Table 2. **Lighting error on rendered scenes.** The columns indicate the splits according to cloudiness (c.f. sec. 4.1), ranging from sunny (su) to overcast (oc), and sunrise/sunset (ss). “all” indicates the average over the entire test set.

energy present in the environment map lowers drastically with clouds occluding the sun.

We can further see the impact of the energy on renders in tab. 2. Similarly to the previous experiment, our method achieves state-of-the-art results. Interestingly, in some categories our method improved upon the results of the LM environment map it received as input, showcasing an advantage in correlating lighting and texture for more scattered illumination configurations. In this table it is also worth highlighting the advantage of LM model’s flexibility, allowing a much more precise parametric fit to the ground truth panoramas. In the first part of the table, all the measures are computed with

respect to the reference ground truth environment map from our test set. Contrarily to parametric models, neither SkyGAN nor our method intend to represent a captured environment map, but instead to preserve the appearance and energy present in their parametric input. As such, the limited expressivity of their parametric input acts as an upper bound for the accuracy of these methods, which we believe to be a small price to pay against the user editability these inputs provide. The second part of tab. 2 presents a comparison of renders against each method’s input, to present more faithfully the capabilities of both methods to preserve the environment map energy. SkyGAN presented visible improvements for clearer skies, possibly due to the parametric model used as input combined with its task of reconstructing the input, but this improvement was not consistent in cloudier skies. Our model improved considerably as more clouds covered the sun, showing again a successful mapping from the clear skies parametric input to all-weather skies.

Qualitative evaluation. We provide visual results from both parametric and learned sky models in fig. 3. Our LM-GAN model yields the most plausible texture in terms of generated clouds for all levels of cloud coverage. While SkyGAN was also able to map different levels of cloud coverage, many artifacts are visible, which is coherent with the results shown in the original article. In this image, the advantage of using the LM model as input is also made clear, as its versatility enables it to emulate different levels of cloud coverage by changing the colors and sun falloffs of its clear skies, almost approximating SkyNet’s auto-encoder results. We further evaluate the dynamic range of the sky models with renders shown in fig. 4. In this experiment, we use the output of each method to light three spheres with different reflectance properties (mirror, Lambertian, glossy), each exhibiting some aspect of the environment: respectively, the texture, energy, and energy falloff around the sun region. In this case, the robustness of our LM fits becomes very clear, being visually enhanced by our model through textures, visible in the reflections.

	metric	LPIPS	LPIPS+GAN	full (ours)
texture	FID	67.09	24.58	20.28
	RMSE	11.11	10.44	10.76
	si-RMSE	10.18	9.04	9.17
ref.	RMSE	1275.40	1094.30	609.94
	si-RMSE	602.24	261.41	122.06
input	RMSE	1215.82	911.99	142.43
	si-RMSE	617.76	261.34	69.65

Table 3. **Ablation errors.** Adding a GAN loss to an LPIPS-based UNet significantly improved visual quality. There was also a significant gain in scale-invariant lighting accuracy, showing the influence texture has on contrast and patterns. Adding a rendering loss helped modulate the remaining lighting loss while improving visual fidelity.

4.3 Ablation studies

To identify the contribution of the individual losses to the final result, we train two other models for the same amount of epochs: one solely on an LPIPS loss [Zhang et al. 2018], the other with LPIPS and the adversarial PatchGAN loss (without the rendering loss). All

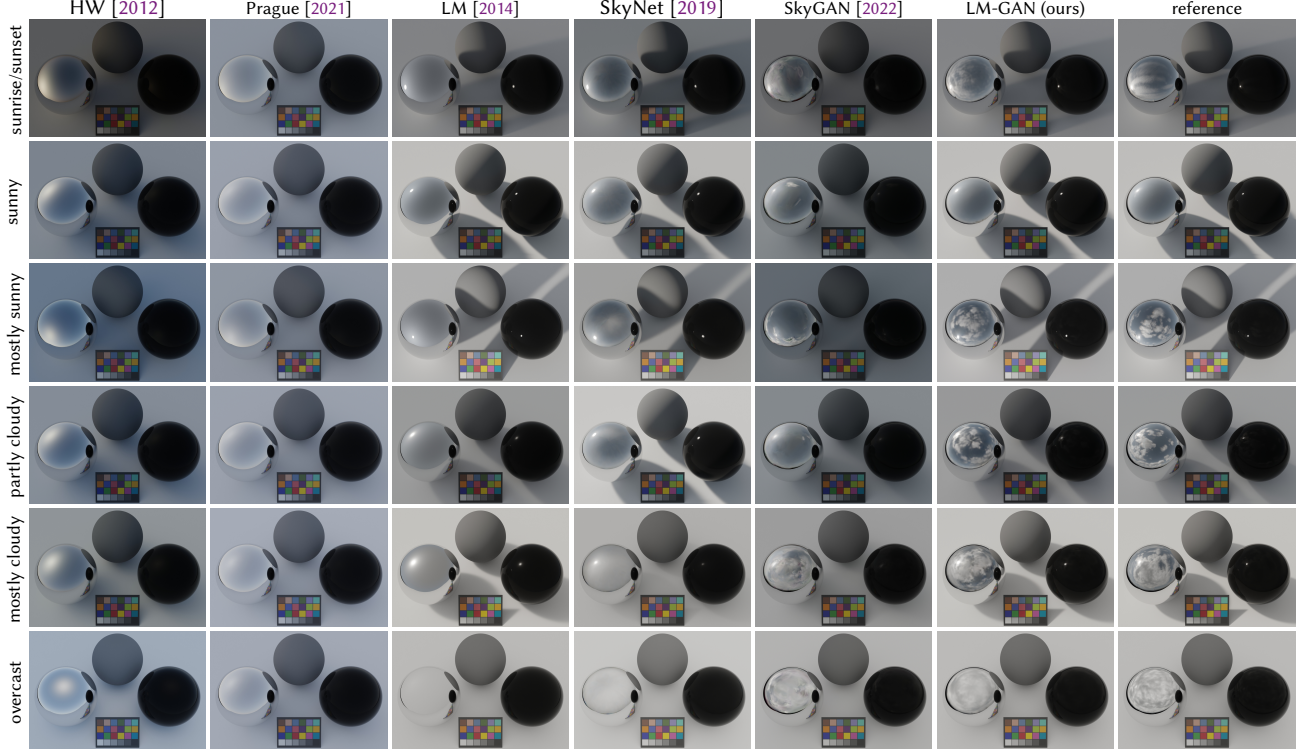


Fig. 4. **Visual comparison of a scene rendered with different lighting models.** Our approach generates high-quality reflections (shiny spheres) while preserving the proper energy (shading and shadows). The peak of HDR energy when the sun is visible can be verified in the black specular spheres.

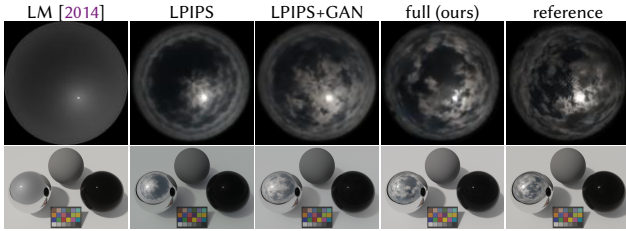


Fig. 5. **Ablation example on a challenging sky.** Using an LPIPS loss (col. 2), the model learns high-frequency cloud textures, but not general structure. A patch discriminator (LPIPS+GAN) improves results (col. 3), but the upper dynamic range is still lost. Adding a rendering loss (full) (col. 4) helps correlate illumination (col. 1) and texture (col. 5).

models were trained at 128×128 resolution. Fig. 5 shows the LPIPS model captures cloud textures locally, repeating it over the image like a pattern, however fails to provide both photorealistic and HDR results. Combining it with PatchGAN is sufficient to achieve a good appearance, but it still struggles to preserve the full HDR, improving only scale-invariant results through proper texture (see tab. tab. 3). Adding a rendering loss further improved the texture and the desired lighting properties, enforcing the desired correlation.

5 CONCLUSION

We present LM-GAN, a learned HDR sky model that generates photorealistic sky environment maps, readily usable for lighting

virtual scenes and objects. Our key contribution lies in the learning of both energy and texture from the sky and the sun simultaneously into a single standalone model, trained directly on real captured skies. Our method is implemented via a rejuvenated yet simple UNet architecture, which is straightforward to implement and efficient to execute. Our proposed model is conditioned on a parametric sky model, which confers both expressivity and physical accuracy to our results. This results in a flexible and user-editable sky model that can be used for several applications.

Despite our state-of-the-art results, our method bears some limitations. First, our method cannot provide the same resolution as professionally captured HDRIs (commonly $12k \times 24k$) due to the limitations of generative machine learning algorithms and the currently available hardware. Also, while our model has several user-editable characteristics such as the sun position and intensity and the color of the sky, our proposed method does not allow for fine-grained control of cloud appearance and location.

We hope our work paves the way for high-quality end-to-end environment modeling which captures the richness of the natural sky, eventually replacing manual artist annotations when lighting 3D scenes or editing images in a photorealistic way.

ACKNOWLEDGEMENTS

This work was supported by NSERC grants ALLRP 557208-20, RGPIN-2020-04799, and Adobe. The authors also thank Nvidia for donating GPUs; Tobias Rittig and Martin Mirbauer for running their Prague sky model fitting code on our dataset; Jinsong Zhang, Henrique Weber, and Aryan Garg for their help with various parts of the code; and Heitor Felix for helpful discussions.

REFERENCES

- Antoine Bouthors, Fabrice Neyret, Nelson Max, Eric Bruneton, and Cyril Crassin. 2008. Interactive multiple anisotropic scattering in clouds. In *Proceedings of the 2008 symposium on Interactive 3D graphics and games*. 173–182.
- Eric Bruneton. 2017. A Qualitative and Quantitative Evaluation of 8 Clear Sky Models. *IEEE Transactions on Visualization and Computer Graphics* 23, 12 (2017), 2641–2655.
- Eric Bruneton and Fabrice Neyret. 2008. Precomputed Atmospheric Scattering. *Computer Graphics Forum* 27, 4 (2008), 1079–1086.
- Paul Debevec. 1998. Rendering synthetic objects into real scenes: Bridging traditional and image-based graphics with global illumination and high dynamic range photography. In *Proc. SIGGRAPH* 98. 189–198.
- Jia Deng, Wei Dong, Richard Socher, Li-Jia Li, Kai Li, and Li Fei-Fei. 2009. Imagenet: A large-scale hierarchical image database. In *IEEE conference on computer vision and pattern recognition*. 248–255.
- Oskar Elek and Petr Knoch. 2010. Real-time spectral scattering in large-scale natural participating media. In *Proceedings of the 26th Spring Conference on Computer Graphics*. 77–84.
- C. Emde, R. Buras-Schnell, A. Kylling, B. Mayer, J. Gasteiger, U. Hamann, J. Kylling, B. Richter, C. Pause, T. Dowling, and L. Bugliaro. 2016. The libRadtran software package for radiative transfer calculations (version 2.0.1). *Geoscientific Model Development* 9, 5 (2016), 1647–1672.
- David Griffiths, Tobias Ritschel, and Julien Philip. 2022. OutCast: Single Image Relighting with Cast Shadows. *Computer Graphics Forum* 41, 2 (2022), 179–193.
- Roger Grosse, Micah K Johnson, Edward H Adelson, and William T Freeman. 2009. Ground truth dataset and baseline evaluations for intrinsic image algorithms. In *2009 IEEE 12th International Conference on Computer Vision*. IEEE, 2335–2342.
- Jörg Haber, Marcus Magnor, and Hans-Peter Seidel. 2005. Physically-based simulation of twilight phenomena. *ACM Transactions on Graphics (TOG)* 24, 4 (2005), 1353–1373.
- Anna Heinle, Andreas Macke, and Anand Srivastav. 2010. Automatic cloud classification of whole sky images. *Atmospheric Measurement Techniques* 3, 3 (2010), 557–567.
- Martin Heusel, Hubert Ramsauer, Thomas Unterthiner, Bernhard Nessler, and Sepp Hochreiter. 2017. GANs Trained by a Two Time-Scale Update Rule Converge to a Local Nash Equilibrium. In *Proceedings of the 31st International Conference on Neural Information Processing Systems* (Long Beach, California, USA) (NIPS’17). 6629–6640.
- Stephen Hill, Stephen McAuley, Laurent Belcour, Will Earl, Niklas Harrysson, Sébastien Hillaire, Naty Hoffman, Lee Kerley, Jasmin Patry, Rob Pieké, Igor Skliar, Jonathan Stone, Pascal Barla, Mégane Bati, and Iliyan Georgiev. 2020. Physically Based Shading in Theory and Practice. In *ACM SIGGRAPH 2020 Courses*. Article 11, 12 pages.
- Štěpán Hojdar. 2019. Using neural networks to generate realistic skies. (2019).
- Yannick Hold-Geoffroy, Akshaya Athawale, and Jean-François Lalonde. 2019. Deep sky modeling for single image outdoor lighting estimation. In *Proceedings of the IEEE/CVF conference on computer vision and pattern recognition*. 6927–6935.
- Yannick Hold-Geoffroy, Kalyan Sunkavalli, Sunil Hadap, Emiliano Gabbaretto, and Jean-François Lalonde. 2017. Deep outdoor illumination estimation. In *Proceedings of the IEEE conference on computer vision and pattern recognition*. 7312–7321.
- Lukáš Hošek and Alexander Wilkie. 2012. An analytic model for full spectral sky-dome radiance. *ACM Transactions on Graphics (TOG)* 31, 4 (2012), 1–9.
- Lukáš Hošek and Alexander Wilkie. 2013. Adding a solar-radiance function to the hošek-wilkie skylight model. *IEEE computer graphics and applications* 33, 3 (2013), 44–52.
- Phillip Isola, Jun-Yan Zhu, Tinghui Zhou, and Alexei A Efros. 2017. Image-to-image translation with conditional adversarial networks. In *Proceedings of the IEEE conference on computer vision and pattern recognition*. 1125–1134.
- Simon Kallweit, Thomas Müller, Brian McWilliams, Markus Gross, and Jan Novák. 2017. Deep Scattering: Rendering Atmospheric Clouds with Radiance-Predicting Neural Networks. *ACM Trans. Graph. (Proc. of Siggraph Asia)* 36, 6, Article 231 (Nov. 2017), 11 pages.
- Tero Karras, Miika Aittala, Samuli Laine, Erik Härkönen, Janne Hellsten, Jaakko Lehtinen, and Timo Aila. 2021. Alias-free generative adversarial networks. In *Advances in Neural Information Processing Systems*.
- Joseph T. Kider, Daniel Knowlton, Jeremy Newlin, Yining Karl Li, and Donald P. Greenberg. 2014. A Framework for the Experimental Comparison of Solar and Skydome Illumination. *ACM Trans. Graph.* 33, 6, Article 180 (nov 2014), 12 pages.
- Diederik P. Kingma and Jimmy Ba. 2015. Adam: A method for stochastic optimization. In *3rd International Conference on Learning Representations, ICLR*.
- JF Lalonde, LP Asselin, J Becirovski, Y Hold-Geoffroy, M Garon, MA Gardner, and J Zhang. 2016. The Laval HDR sky database.
- Jean-François Lalonde and Iain Matthews. 2014. Lighting estimation in outdoor image collections. In *2014 2nd International Conference on 3D Vision*, Vol. 1. IEEE, 131–138.
- Martin Mirbauer, Tobias Rittig, Tomáš Iser, Jaroslav Krivánek, and Elena Šikudová. 2022. SkyGAN: Towards realistic cloud imagery for image based lighting. In *Eurographics Symposium on Rendering*. The Eurographics Association.
- Parry Moon. 1940. Proposed standard solar-radiation curves for engineering use. *Journal of the Franklin Institute* 230, 5 (1940), 583–617.
- Tomoyuki Nishita, Yoshinori Dobashi, and Eihachiro Nakamae. 1996. Display of clouds taking into account multiple anisotropic scattering and sky light. In *Proceedings of the 23rd annual conference on Computer graphics and interactive techniques*. 379–386.
- Tomoyuki Nishita, Takao Sirai, Katsumi Tadamura, and Eihachiro Nakamae. 1993. Display of the earth taking into account atmospheric scattering. In *Proceedings of the 20th annual conference on Computer graphics and interactive techniques*. 175–182.
- National Oceanic and Atmospheric Administration. 2023. *Forecast Terms*. https://www.weather.gov/bgm/forecast_terms
- Sean O’Neil. 2005. Accurate atmospheric scattering. *Gpu Gems* 2 (2005), 253–268.
- Richard Perez, Robert Seals, and Joseph Michalsky. 1993. All-weather model for sky luminance distribution—preliminary configuration and validation. *Solar energy* 50, 3 (1993), 235–245.
- Arco J Preetham, Peter Shirley, and Brian Smits. 1999. A practical analytic model for daylight. In *Proceedings of the 26th annual conference on Computer graphics and interactive techniques*. 91–100.
- Erik Reinhard, Wolfgang Heidrich, Paul Debevec, Sumanta Pattanaik, Greg Ward, and Karol Myszkowski. 2010. *High dynamic range imaging: acquisition, display, and image-based lighting*. Morgan Kaufmann.
- Olaf Ronneberger, Philipp Fischer, and Thomas Brox. 2015. U-net: Convolutional networks for biomedical image segmentation. In *International Conference on Medical image computing and computer-assisted intervention*. Springer, 234–241.
- Pinar Satilmis, Demetris Marnerides, Kurt Debattista, and Thomas Bashford-Rogers. 2022. Deep Synthesis of Cloud Lighting. *IEEE Computer Graphics and Applications* (2022).
- Karen Simonyan and Andrew Zisserman. 2015. Very deep convolutional networks for large-scale image recognition. In *3rd International Conference on Learning Representations, ICLR*.
- Peter-Pike Sloan, Jan Kautz, and John Snyder. 2002. Precomputed radiance transfer for real-time rendering in dynamic, low-frequency lighting environments. In *Proceedings of the 29th annual conference on Computer graphics and interactive techniques*. 527–536.
- Nitish Srivastava, Geoffrey Hinton, Alex Krizhevsky, Ilya Sutskever, and Ruslan Salakhutdinov. 2014. Dropout: a simple way to prevent neural networks from overfitting. *The journal of machine learning research* 15, 1 (2014), 1929–1958.
- Jessi Stumpf, Andrew Jones, Andreas Wenger, Chris Tchou, Tim Hawkins, and Paul Debevec. 2006. Direct HDR Capture of the Sun and Sky. In *ACM SIGGRAPH 2006 Courses*. 5–es.
- Petr Vévoda, Tom Bashford-Rogers, M Kolářová, and Alexander Wilkie. 2022. A Wide Spectral Range Sky Radiance Model. (2022).
- Alexander Wilkie, Petr Vévoda, Thomas Bashford-Rogers, Lukáš Hošek, Tomáš Iser, Monika Kolářová, Tobias Rittig, and Jaroslav Krivánek. 2021. A fitted radiance and attenuation model for realistic atmospheres. *ACM Transactions on Graphics (TOG)* 40, 4 (2021), 1–14.
- Piaopiao Yu, Jie Guo, Fan Huang, Cheng Zhou, Hongwei Che, Xiao Ling, and Yanwen Guo. 2021a. Hierarchical Disentangled Representation Learning for Outdoor Illumination Estimation and Editing. In *Proceedings of the IEEE/CVF International Conference on Computer Vision*. 15313–15322.
- Piaopiao Yu, Jie Guo, Longhai Wu, Cheng Zhou, Mengtian Li, Chenchen Wang, and Yanwen Guo. 2021b. Dual attention autoencoder for all-weather outdoor lighting estimation. *Sci. China Inf. Sci.* 64 (2021).
- Hongyi Zhang, Yann N Dauphin, and Tengyu Ma. 2019a. Fixup initialization: Residual learning without normalization. *arXiv preprint arXiv:1901.09321* (2019).
- Jinsong Zhang, Kalyan Sunkavalli, Yannick Hold-Geoffroy, Sunil Hadap, Jonathan Eisenman, and Jean-François Lalonde. 2019b. All-weather deep outdoor lighting estimation. In *Proceedings of the IEEE/CVF Conference on Computer Vision and Pattern Recognition*. 10158–10166.
- Richard Zhang, Phillip Isola, Alexei A Efros, Eli Shechtman, and Oliver Wang. 2018. The unreasonable effectiveness of deep features as a perceptual metric. In *Proceedings of the IEEE conference on computer vision and pattern recognition*. 586–595.